**Titania-silver and alumina-silver composite nanoparticles: novel, versatile synthesis, reaction mechanism and potential antimicrobial application**

Tanushree Bala [a], Gordon Armstrong [b*], Fathima Laffir [c] and Roibeard Thornton [d]

Materials & Surface Science Institute, University of Limerick, Limerick, Ireland.

[a] email: tanushree31@yahoo.co.in

[b] email: gordon.armstrong@ul.ie

[c] email : fathima.laffir@ul.ie

[d] email: roibeard.thornton@ul.ie

*To whom correspondence should be addressed. Tel +353-61-213127, Fax +353-61-213529.

**Abstract**

Titania–silver ($TiO_2$–Ag) and alumina–silver ($Al_2O_3$–Ag) composite nanoparticles were synthesised by a simple, reproducible, wet chemical method under ambient conditions. The surface of the oxides was modified with oleic acid, which acted as an intermediate between the oxide surface and the silver nanoparticles. The resulting composite nanoparticles were thoroughly characterized by XRD, TEM, XPS, FTIR and TGA to elucidate the mode of assembly of Ag nanoparticles on the oxide surfaces. Epoxy nanocomposites were formulated with $TiO_2$–Ag and $Al_2O_3$–Ag to examine potential applications for the composite nanoparticles. Preliminary results from disk diffusion assays against *Escherichia coli* DH5α and *Staphylococcus epidermidis* NCIMB 12721 suggest that these $TiO_2$–Ag and $Al_2O_3$–Ag composite nanoparticles have potential as antimicrobial materials.

Keywords: $TiO_2$–Ag, $Al_2O_3$–Ag, composite, nanoparticle, epoxy polymer, antimicrobial, *Staphylococcus epidermidis*, *Escherichia coli.*

## 1. Introduction

Significant research effort is directed towards bottom-up synthesis of composite nanomaterials which combine the properties of two or more materials in a single product. Numerous reports describe the synthesis of such composite materials, with particular emphasis on immobilization of noble metal nanoparticles on oxides such as $SiO_2$ [1-3], $TiO_2$ [4-10] and $Al_2O_3$ [11-16]. These oxides are of interest due to their ready availability, ease of handling, low toxicity and low cost. They offer favourable mechanical strength, thermal stability, high surface area, and - very importantly - allow adsorption of various solids and organic ligands on their surface.

For the latter reason, $Al_2O_3$ has been extensively exploited as an adsorbent for waste water treatment [17], as a molecular sieve [18] and in nanoparticle-based catalysis. Ni [11], Pt [12], Pd [13], Ru [14] and CuO [16] are among the numerous species that have been studied to produce $Al_2O_3$-based catalysts. As an excellent adsorbent, $TiO_2$ also enjoys a vast range of potential applications in photocatalysis [4-6], photovoltaics [7, 8] and water splitting [9], either in its pristine form or as a composite with a variety of nanoparticles. Noble metals including Au [19] and Ag [20, 21], magnetic particles such as Ni [22] and ferrites [23], quantum dots [24], hydroxyapatites [25] and various oxides (e.g. alumina [26], zirconia [27], silica [28] and NiO [29]) have been successfully incorporated on titania particles, rods, wires or mesh-like structures. $TiO_2$-Ag has attracted particular attention for its non-toxic nature [30], catalytic activity [31, 32] and shape-dependent optical properties under visible light [33, 34]. Moreover the material could also achieve enhanced photocatalytic efficiency [35]. Thus, a facile and reproducible synthetic route to $TiO_2$-Ag and $Al_2O_3$-Ag composite nanoparticles would be useful in a diverse range of applications.

Here we report a wet chemical based synthesis to produce $TiO_2$-Ag and $Al_2O_3$-Ag composite nanoparticles, followed by their incorporation in epoxy polymer for evaluation as antimicrobial materials. A primary objective of the current study was to synthesise composite nanoparticles with controllable, reproducible morphologies. The method reported here gave products with consistent properties in high yield under ambient conditions using only using simple apparatus unlike many other reported procedures [36, 37]. These composite nanoparticles were easily dispersed in common laboratory solvents, allowing them to be readily incorporated in polymer resins as functional additives.

To demonstrate a potential application for these novel materials, the composite nanoparticles were used to formulate epoxy polymer nanocomposites; these polymer nanocomposites were tested for antimicrobial activity. There is growing interest in antimicrobial materials, driven by an urgent need for more effective strategies to control microbial infection. However, as increasing frequency of antibiotic resistance makes it ever more difficult to treat such infections, new and more effective antimicrobial strategies and materials are required. One such strategy is to break the chain of infection by incorporation of antimicrobial substances into contact surfaces. Silver is recognised for its antimicrobial activity in a variety of physiological settings. Silver ions form metal-organic complexes with sulfhydryl groups on outer cell walls of bacteria and fungi, thereby inactivating enzymes critical for energy metabolism and electron transport [36].

## 2. Materials and methods

**Chemicals**. Titanium dioxide ($TiO_2$), aluminium oxide ($Al_2O_3$), oleic acid (cis-9-octadecenoic acid, $C_{17}H_{33}COOH$), anhydrous methanol, silver nitrate ($AgNO_3$), sodium borohydride ($NaBH_4$), bisphenol A propoxylate (1PO/phenol)diglycidyl ether (epoxy resin) and diethylenetriamine (hardener) were obtained from Sigma Aldrich. All reagents were > 99 % purity and were used as received.

**Synthesis.** 1 g of $TiO_2$ or $Al_2O_3$ powder was stirred with 10 ml of $1X10^{-2}$ M oleic acid in methanol at 500 rpm on a magnetic stirrer at room temperature until evaporation. 10 ml of $1X10^{-2}$ M aqueous $AgNO_3$ solution, sufficient to yield a final loading of silver nanoparticles of 1 wt% (calculated with respect to the initial mass of oxide), was added to the dried sample. The reaction vessel was covered with aluminium foil to exclude light, then stirred overnight. 0.004 g $NaBH_4$ powder was added with stirring; immediately the white suspension of the reaction mixture changed to grey. The product was dried thoroughly on a hot-plate at 100 ºC, then washed with copious amounts of water, followed by ethanol, to remove unreduced precursors and any Ag nanoparticles if formed separately.

Also, a repeat experiment was conducted as above in which the sample was washed with ethanol after addition of oleic acid to remove uncoordinated oleic acid, to better understand the coordination of oleic acid with the oxide surfaces during the synthesis.

To prepare composite nanoparticles with 10 wt% Ag loading on the oxides, the above process was repeated using $1X10^{-1}$ M $AgNO_3$ solution and 0.04 g of $NaBH_4$ in the appropriate steps.

Polymer nanocomposites were prepared by dispersing the composite nanoparticles synthesised above in epoxy resin at 1, 10, 30 and 50 wt% loading. The required loading of nanoparticle was mixed with 1 g epoxy resin (e.g. 0.01 g nanoparticles were mixed with 1 g of epoxy resin to yield 1 wt% loading) by stirring on a magnetic stirrer overnight. 0.1 g of hardener was added to the mixture, stirred for a further 5 minutes, then placed in a PTFE mould and placed in an oven at 90 ºC until completely cured.

**Characterisation.** *Transmission electron microscopy (TEM)*. TEM images were obtained on a JEOL JEM 2011 microscope at an accelerating voltage at 200 kV. Samples were prepared by placing a drop of the solutions to be examined on 300 mesh carbon-coated copper grids. These films were allowed to dry for 2 minutes, after which excess solution was removed using blotting paper. TEM samples of polymer nanocomposites were prepared by scraping the top layer of the free-standing composite with a scalpel and transferring the scrapings onto a 300 mesh carbon-coated copper grid.

*X-ray photo electron spectroscopy (XPS).* XPS was performed on a Kratos AXIS 165 spectrometer using monochromatic Al Kα radiation of energy 1486.6 eV. High resolution spectra of C 1s, O 1s, Ti 2p, Al 2p and Ag 3d were taken at a fixed pass energy of 20 eV, 0.05 eV step size and 100 ms dwell time per step. Surface charge was efficiently neutralised by flooding the sample surface with low energy electrons. Core level binding energies were corrected using the C 1s peak at 284.8 eV as the charge reference. For construction and fitting of synthetic peaks of high resolution spectra, a mixed Gaussian-Lorenzian function with a Shirley type background subtraction were used.

*Attenuated total reflectance infrared spectroscopy (ATR-IR).* Infrared spectra were recorded on a Perkin Elmer Spectrum-One spectrometer fitted with a Universal ATR (attenuated total reflectance) accessory. Each spectrum presented is the average of 16 scans recorded at a resolution of 4 $cm^{-1}$. The spectra were normalised against the strongest peak observed (2925 $cm^{-1}$) to allow reliable

comparisons of relative peak intensity and plotted using Perkin Elmer Spectrum ES v.6.3 software. No other corrections were applied to the data.

*X-ray powder diffraction (XRD).* XRD was conducted on a Philips X'Pert PRO MPD fitted with a Cu Kα radiation source operating at 40 kV and a current of 30 mA. A step size of 0.020 º 2θ and collection time of 1second per step was used for all experiments. Diffraction patterns were analysed using Philips X'Pert HighScore Plus v.2.2.b software with the International Centre for Diffraction Data (ICDD) Release 2007 RDB.

*Thermogravimetric analysis (TGA).* TGA was conducted on a Perkin Elmer TGA1 thermogravimetric analyser. Samples were heated from 30 ºC to 900 ºC at a ramp rate of 10 $K.min^{-1}$ in flowing nitrogen atmosphere. The average sample mass was 6 mg.

*Antimicrobial testing.* The antibacterial activity of the discs was evaluated against both Gram negative and Gram positive species including *Escherichia coli* DH5α (*E. coli*) and *Staphylococcus epidermidis* NCIMB 12721 (*S. Epidermidis*) using the agar disc-diffusion method [37]. Luri Bertani (LB) agar and broth were used for culturing *E. coli*. *S. epidermidis* was cultured in Brain hearth infusion (BHI) broth and agar. All organisms were grown aerobically with agitation at 37 ºC. Agar plates were seeded with both cultures, then 3 discs (6 mm diameter) of each material were embedded into the surface of the plates. Overnight bacterial cultures (1:100 dilution) were streak plated onto the surface of the agar plates using a sterile swab and incubated overnight at 37 ºC. Callipers were used to measure zones of inhibition.

**3. Results and discussion**

The formation of Ag nanoparticles on the titania and alumina surfaces was confirmed by XRD, as shown in Figure 1. The titania starting material was the anatase phase of the oxide (cf. Curve 1, Figure 1A; ICDD Ref. code 03-065-5714). The alumina starting material was the alpha phase of the oxide (cf. Curve 1, Figure 1B; ICDD Ref. code 01-070-5679). In both cases, the appearance of fcc Ag peaks (JCPDS file no. 04-0783) after reducing $Ag^{+}$ ions on the oxide surfaces (cf. Curve 2, Figure 1A; Curve 2, Figure 1B) indicated that Ag nanoparticles were present on the oxide surfaces.

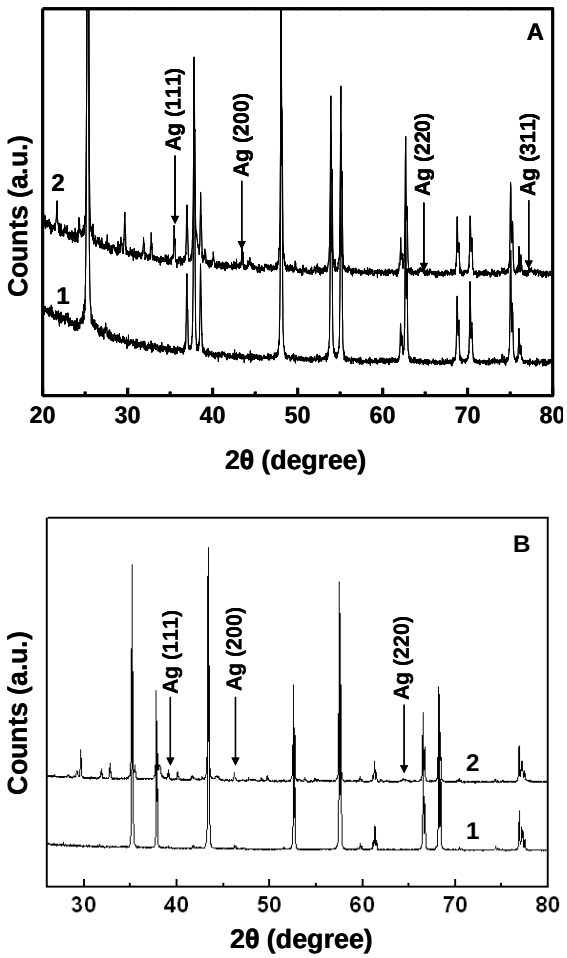


**Figure 1.** (A) XRD pattern of pristine titania (Curve 1) and $TiO_2$–Ag composite nanoparticles (Curve 2). The peaks attributed to Ag nanoparticles are in agreement with fcc crystal structure; (B) XRD pattern of pristine alumina (Curve 1) and $Al_2O_3$–Ag composite nanoparticles (Curve 2). The Ag peaks and the corresponding planes are arrowed.

The TEM micrographs presented in Figure 2 illustrates the formation of Ag nanoparticles on the surface of $TiO_2$ and $Al_2O_3$ nanoparticles along with the pristine oxides. Figure 2A and 2D show pristine $TiO_2$ (particle size: 130 - 200 nm) and $Al_2O_3$ (particle size range: 100 - 200 nm). In both cases, the Ag nanoparticles formed were not of uniform size. Though the majority of these particles were spherical in shape, non-spherical morphologies were also observed. Ag nanoparticles were observed as discrete particles on the surface of the $TiO_2$ particles (cf. Figure 2B); they were most prominent under dark field imaging (cf. Figure 2C) in which the more crystalline Ag nanoparticles were observed as scintillating spots over the less crystalline $TiO_2$ particles.

However, in case of $Al_2O_3$ support, all the Ag nanoparticles were not well localized on the support; unbound Ag nanoparticles were also observed in the $Al_2O_3$–Ag samples (cf. Figure 2E, 2F). Although both samples were prepared following the same procedure, these observations suggest that the Ag nanoparticles were formed following different modes of assembly, probably due to a difference in co-ordination of the oleic acid ligand on the surface of the two different oxides. Therefore, XPS, FTIR and TGA experiments were conducted on both to confirm the presence of silver on the titania and alumina surfaces and to elucidate the modes of assembly that may account for the differences observed in the final composite nanoparticles.

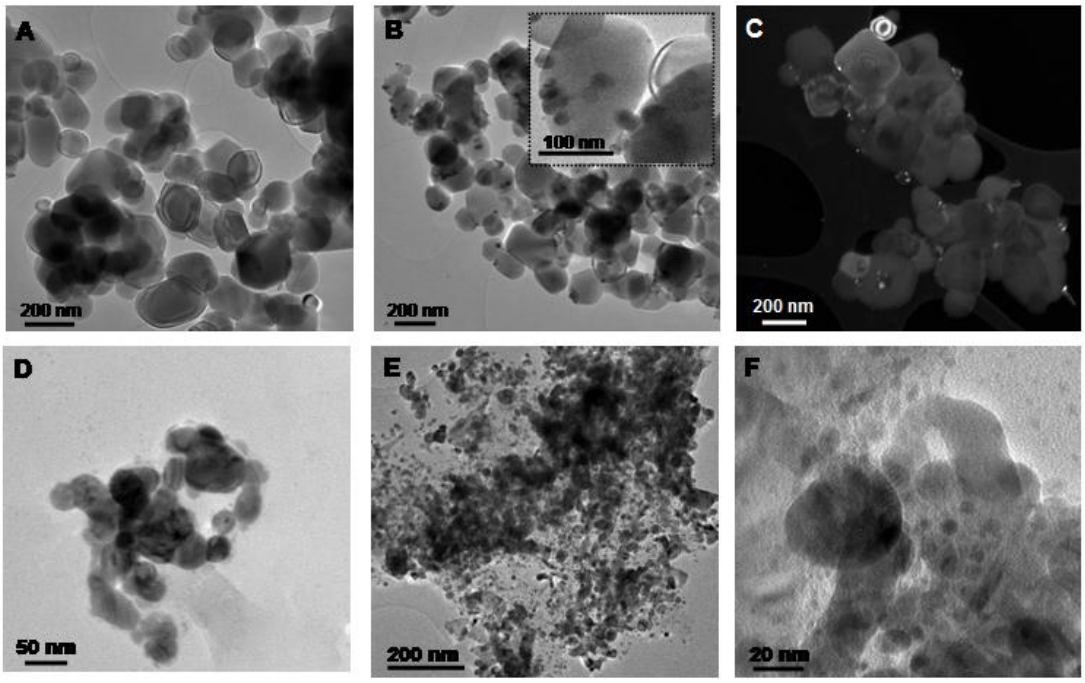


**Figure 2.** (A) TEM image of pristine titania nanoparticles. (B, C) TEM images of Ag nanoparticles on titania surface. (D) TEM image of pristine alumina particles. (E, F) TEM images of Ag nanoparticles on alumina surface.

**Characterisation of $TiO_2$–Ag composite nanoparticles.** The formation of Ag nanoparticles on titania was further confirmed by XPS. Figures 3A-D show the C 1s, O 1s, Ti 2p and Ag 3d spectra, respectively, of the $TiO_2$–Ag composite nanoparticles. The C 1s peak appeared at 284.8 eV along with two minor components at 286.5 eV and 288.8 eV which could be attributed to C-C/C-H of hydrocarbons or adventitious carbon, C–O and –COO type of bonding present in oleic acid respectively. The O 1s peak could be fitted with three components. The main component at 529.5 eV corresponded to Ti-O in $TiO_2$. The minor components were attributed to O from oxygenated carbon

species including carboxylic acid groups of oleic acid. The Ti 2p spectra appeared as a doublet with Ti $2p_{3/2}$ peak at 458.7 eV and doublet separation of 5.7 eV, characteristic of $TiO_2$ [38-40]. The Ag 3d spectra appeared as doublet of narrow peaks (fwhm = 0.9 eV) with Ag $3d_{5/2}$ at a binding energy of 368.0 eV and doublet separation of 6.0 eV. These values corresponded to metallic silver [40, 41] and were further indicative that all the ions were successfully reduced with sodium borohydride during the formation of Ag nanoparticles.

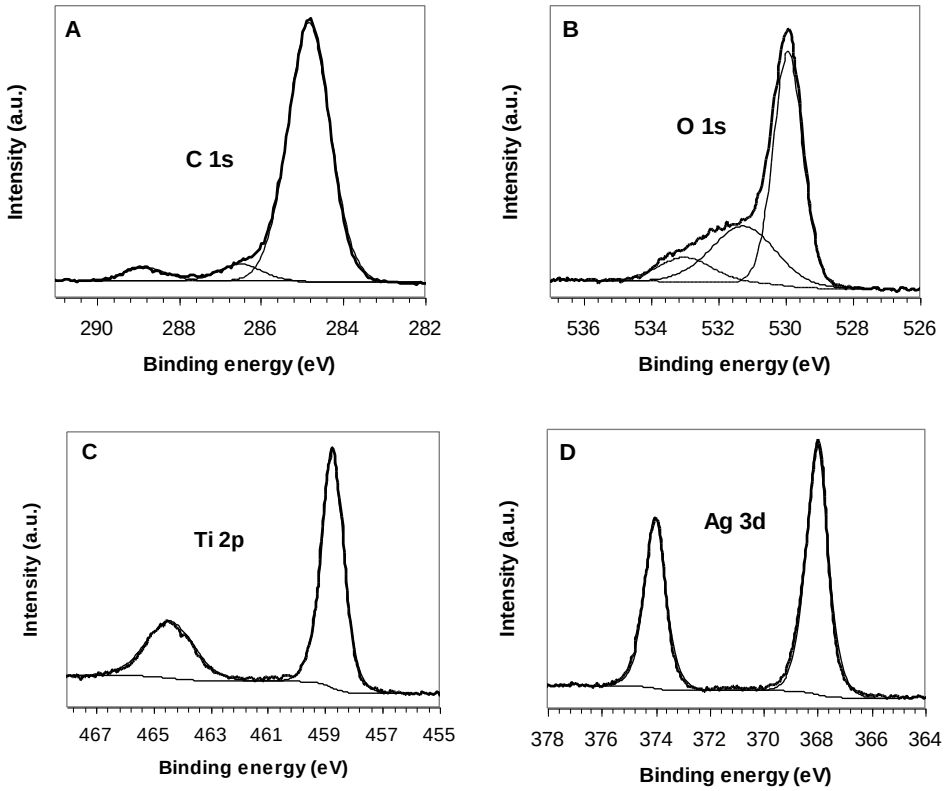


**Figure 3.** (A) C 1s, (B) O 1s, (C) Ti 2p, (D) Ag 3d X-ray photoelectron spectra obtained for $TiO_2$–Ag composite nanoparticles.

A significant increase in carbon content was noted when compared to the carbon composition of pristine titania due to presence of oleic acid (cf. Figure SI-1, Supporting Information). Though the XPS study suggested bonding of the oleic acid with the $TiO_2$ surface and formation of Ag nanoparticles, it could not clearly reveal the mechanism of such interactions. Infrared spectroscopy conducted at each step of the synthesis (cf. Figure 4), proved more informative in determining the mode of assembly of $TiO_2$–Ag composite nanoparticles. A detailed assignment of the infrared spectrum of neat oleic acid is presented in Figure SI-2, Supporting Information.)

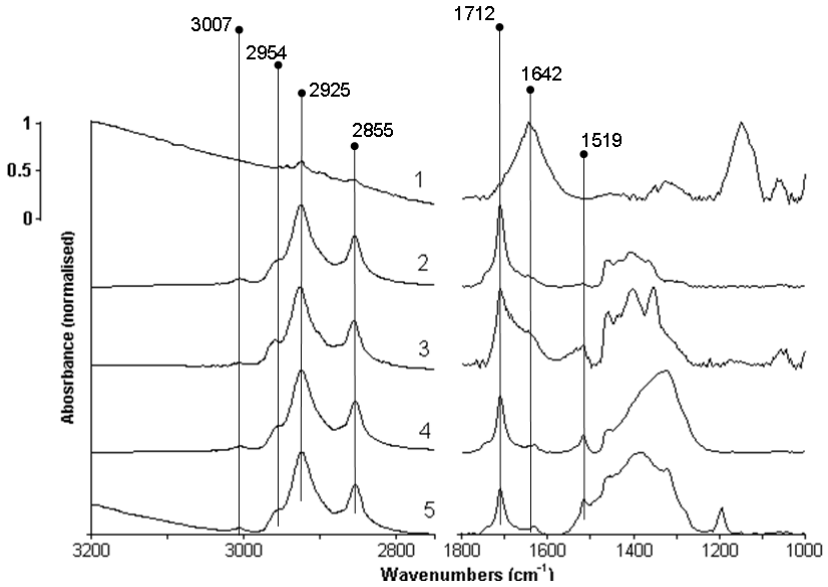


**Figure 4.** Normalised ATR-IR spectra obtained at each stage of $TiO_2$–Ag composite nanoparticle synthesis. (1) Pristine titania; (2) after treatment with oleic acid; (3) following ethanol wash to remove un-coordinated oleic acid molecules; (4) titania-oleic acid after interaction with $Ag^+$; (5) titania-oleic acid after formation of Ag nanoparticles. The spectra have been displaced vertically along the Y axis for clarity; the scale bar shows the peak intensity of each spectrum presented.

Curve 1, Figure 4 shows the spectrum obtained for pristine $TiO_2$, which exhibited a single significant peak at 1642 $cm^{-1}$, in good agreement with previous data [42]. Upon addition of oleic acid/methanol dispersion to titania, the appearance of peaks at 2855 and 2925 $cm^{-1}$ and a shoulder at 2954 $cm^{-1}$ confirmed the presence of oleic acid on the $TiO_2$ surface (cf. Curve 2, Figure 4) [43]. Additional peaks were observed at 1712 $cm^{-1}$ (undissociated -COOH) and 3007 $cm^{-1}$ (olefinic C-H stretching). It has previously been hypothesised that oleic acid adsorbs on the surface of the Lewis acid $TiO_2$ [43].

In a repeat synthesis, the sample was washed with ethanol after addition of oleic acid to remove uncoordinated oleic acid. Curve 3, Figure 4, shows the infrared spectrum obtained from the sample after this additional washing step. No appreciable change in the significant peaks of the spectrum was observed by comparison to Curve 2, Figure 4.

After addition of $AgNO_3$, a new peak was observed at 1519 $cm^{-1}$ (cf. Curve 4, Figure 4). This was considered evidence that $Ag^+$ ions were interacting with the -COOH groups of oleic acid to form an Ag-

oleate complex [44-46]. The 1519 $cm^{-1}$ peak remained following the reduction of $Ag^+$ complex with $NaBH_4$ (cf. Curve 5, Figure 4A), which indicated that the formation of Ag nanoparticles did not affect the adsorbed oleic acid and thus helped Ag nanoparticles to adhere to titania.

These findings are illustrated in Scheme 1. This shows how oleic acid molecules adsorbed on the titania surface via their electron-rich double bonds. The pH before addition of $NaBH_4$ was 4.26, further supporting this hypothesis: Oleic acid molecules have previously been reported to attach with titania through its olefinic centre at acidic pH [43]. It was concluded that $Ag^+$ ions coordinated to the relatively free –COOH groups, then Ag nanoparticles formed on the surface of the $TiO_2$ particles with the oleic acid acting as a linker between the titania and Ag nanoparticles. These conclusions are in agreement with previous reports, since oleic acid is a well-known capping agent for Ag nanoparticles [44-46].

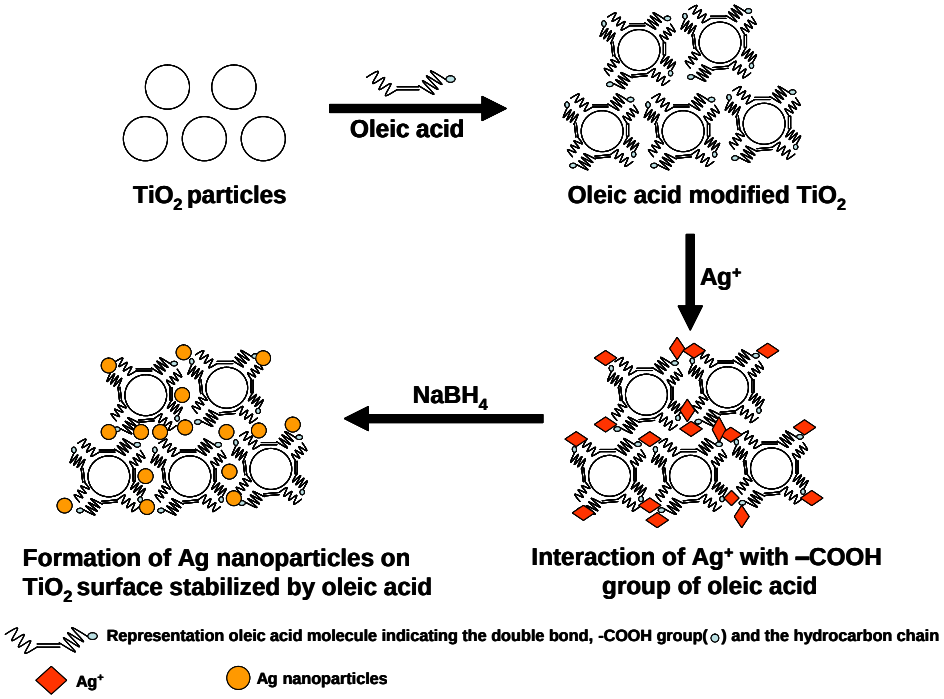


**Scheme 1.** Mode of assembly of $TiO_2$–Ag composite nanoparticles. The role of oleic acid in the synthesis is indicated.

**Characterisation of $Al_2O_3$–Ag composite nanoparticles:** The mode of assembly of $Al_2O_3$–Ag composite nanoparticles was determined by a detailed XPS and ATR-IR study following the same rationale used for $TiO_2$–Ag.

Figures 5A-D show the C 1s, O 1s, Al 2p and Ag 3d spectra, respectively, of $Al_2O_3$–Ag composite nanoparticles. The main C 1s peak at 284.8 eV corresponded to C–C/C–H of hydrocarbons or

adventitious carbon showing an appreciable increase in intensity resulting from the addition of oleic acid. The two minor components were ascribed to C–O and –COO type groups. The O 1s spectrum in Figure 5B showed a main peak at 531.2 eV which was identified as O from alumina. The Al 2p peak appeared at a binding energy of 74.4 eV, accompanying a shift of 0.5 eV from Al 2p in neat alumina which was at 73.9 eV (cf. Figure SI-3, Supporting Information). The latter binding energy (73.9 eV) was comparable to a hydrated alumina surface or $Al(OH)_3$ [44]. The shift in binding energy was probably caused by the adsorption of –COOH groups to the surface and the resulting binding energy was comparable to bulk $Al_2O_3$ [44, 47]. Ag 3d spectra (cf. Figure 5D) had Ag $3d_{5/2}$ and Ag $3d_{3/2}$ at 368.3 and 374.3 eV respectively. Doublet peaks were narrow with fwhm of 1.0 eV and had a separation of 6 eV, characteristic of metallic silver [48]. This confirmed that $Ag^+$ ions were successfully reduced with sodium borohydride. The XPS spectra obtained from neat and oleic acid–modified alumina are presented in Supporting Information, Figure SI-3 for comparison.

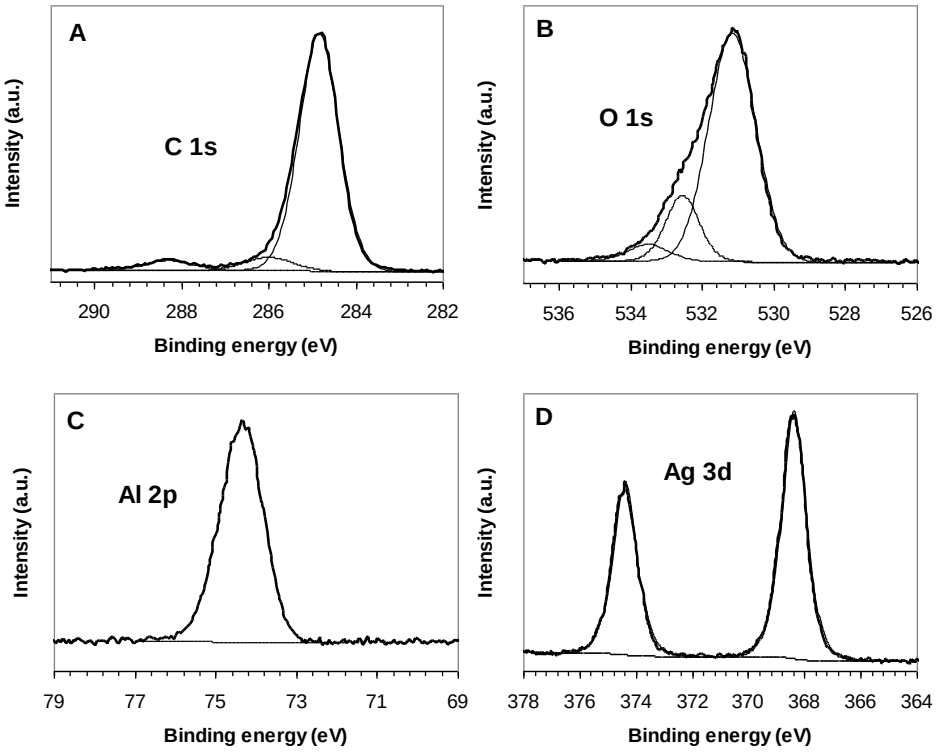


**Figure 5.** (A) C1s, (B) O1s, (C) Al2p and (D) Ag3d X-ray photoelectron spectra obtained for $Al_2O_3$-Ag composites.

Curve 1, Figure 6 shows the infrared spectrum obtained for pristine alumina. No significant bands were observed, consistent with previous reports [49]. Upon addition of oleic acid/methanol dispersion, no band shift was detected in the region 3010–2850 $cm^{-1}$ (cf. Curve 2, Figure 6). This suggested that oleic acid did not interact with alumina through its electron rich olefinic bond, as was observed for titania. A broad band in the region 1470–1410 $cm^{-1}$ was assigned to $CH_2$ bending and C–O–H in-plane bending. The peak at 1291 $cm^{-1}$ was assigned to C-OH stretching.

Carboxylic acids tend to form hydrogen-bonded dimers in both the liquid and solid state [50]. Whereas the C=O stretching vibration occurs around 1760 $cm^{-1}$ for monomeric COOH, it is typically observed at lower frequency for COOH dimers. Therefore, the band at 1746 $cm^{-1}$ was attributed to a shifted peak for the free COOH group, suggesting that some strong interaction occurred between oleic acid and the alumina surface. The stronger band observed at 1707 $cm^{-1}$ was attributed to hydrogen-bonded COOH. Considered together, these observations suggested the formation of a bi-layer by oleic acid moieties. These conclusions are consistent with those reported by Dablemont *et al* for the interaction of carboxylate-functionalised Pt nanoparticles with alumina [49].

As for the $TiO_2$–Ag synthesis, a repeat $Al_2O_3$-Ag synthesis was conducted in which the sample was washed with ethanol after addition of oleic acid to remove uncoordinated oleic acid. Curve 3, Figure 6, shows the infrared spectrum obtained from the sample after this additional washing step. No change to the infrared spectrum was observed after washing the sample with ethanol to remove any uncoordinated oleic acid present (cf. Curve 3, Figure 6), which is further evidence of strong interaction. This kind of interaction is more probable at lower pH when the –COOH groups were expected in their un-dissociated form. In the present synthesis, the pH of the solution before borohydride addition was found to be 5.25.

The infrared spectrum changed appreciably after the addition of AgNO3 (cf. Curve 4, Figure 6). Ag+ ions coordinated with the –COOH groups of the outer layer of the oleic acid bilayer present on the alumina surface. A new peak was observed at 1522 cm-1, attributed to the formation of an Ag-oleate complex with the -COOH groups of the second layer of oleic acid (cf. Curve 4, Figure 6) [44-46]. Further changes were observed in the infrared spectrum after reduction with NaBH4 (cf. Curve 5,

Figure 6). After addition of NaBH4 the pH of the solution changed to 8.4,7 which converted the –COOH groups of the inner layer of oleic acid interacting directly with the alumina surface into –COO - groups. Thus, both the peaks at 1707 and 1746 cm-1 were replaced by a single -C=O band at 1522 cm-1 in Curve 5, Figure 6. No such change was observed during the TiO2-Ag composite synthesis, since the interaction was through the olefinic centre.

The mode of assembly for $Al_2O_3$-Ag composite nanoparticles was found to be in good agreement with that reported by Kasprzyk-Hordern et al [18]. Moreover, in addition to shifting the pH to 9.26, the $Ag^+$ ions were reduced due to addition of $NaBH_4$. Thus it could be concluded that oleic acid coordinated with the Ag nanoparticles through its head groups, as oleic acid is a well-known capping agent for Ag nanoparticles [44-46]. No significant shift was observed in the region 3010-2850 $cm^{-1}$ throughout the synthesis (cf. curves 3-5, Figure 6), indicating that the olefinic bond remained unaltered throughout the reaction.

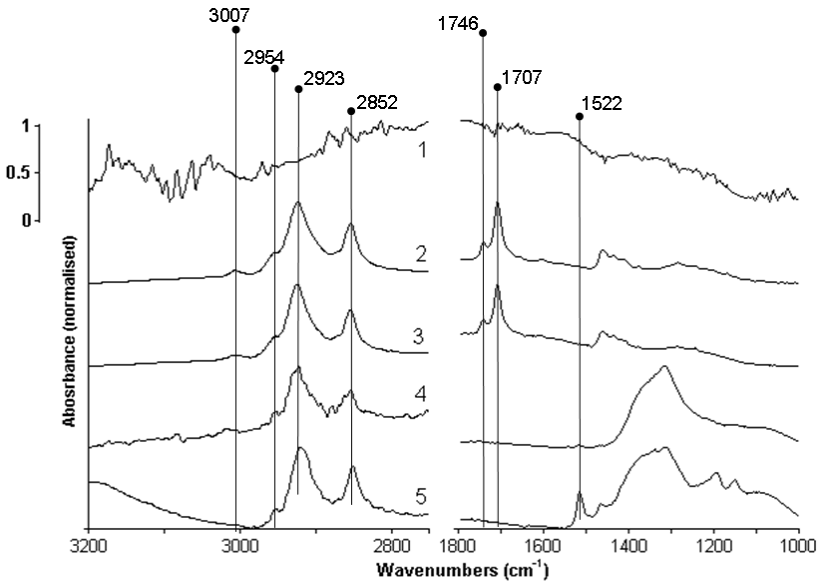


**Figure 6.** Normalised ATR-IR spectra obtained at each stage of $Al_2O_3$–Ag composite nanoparticle synthesis. (1) Pristine alumina; (2) after treatment with oleic acid; (3) following ethanol wash to remove un-coordinated oleic acid molecules; (4) alumina-oleic acid after interaction with $Ag^+$; (5) alumina-oleic acid after formation of Ag nanoparticles. The spectra have been displaced vertically along the Y axis for clarity; the scale bar shows the peak intensity of each spectrum presented.

The proposed mode of assembly for $Al_2O_3$–Ag composite nanoparticles is presented in Scheme 2. Initially, the surface was rich in hydroxyl groups (cf. Scheme 2A), a signature for $Al(OH)_3$ was observed by XPS (cf. Figure SI-3C, Supporting Information). At the first step of the reaction the oleic acid interacted with the surface through its free carboxylic functional group, a clear indication of which was observed by ATR-IR (cf. Scheme 2B). The presence of two carboxylic bands suggested the formation of double layer structures. $Ag^+$ addition and subsequently $NaBH_4$ reduction occurred in the next two steps. The formation of Ag nanoparticles and the role of oleic acid at these steps are clearly shown in Scheme 2C and 2D. $Ag^+$ ions, which were bound to the outer oleic acid layer, were reduced to form nanoparticles that remained bound to the surface.

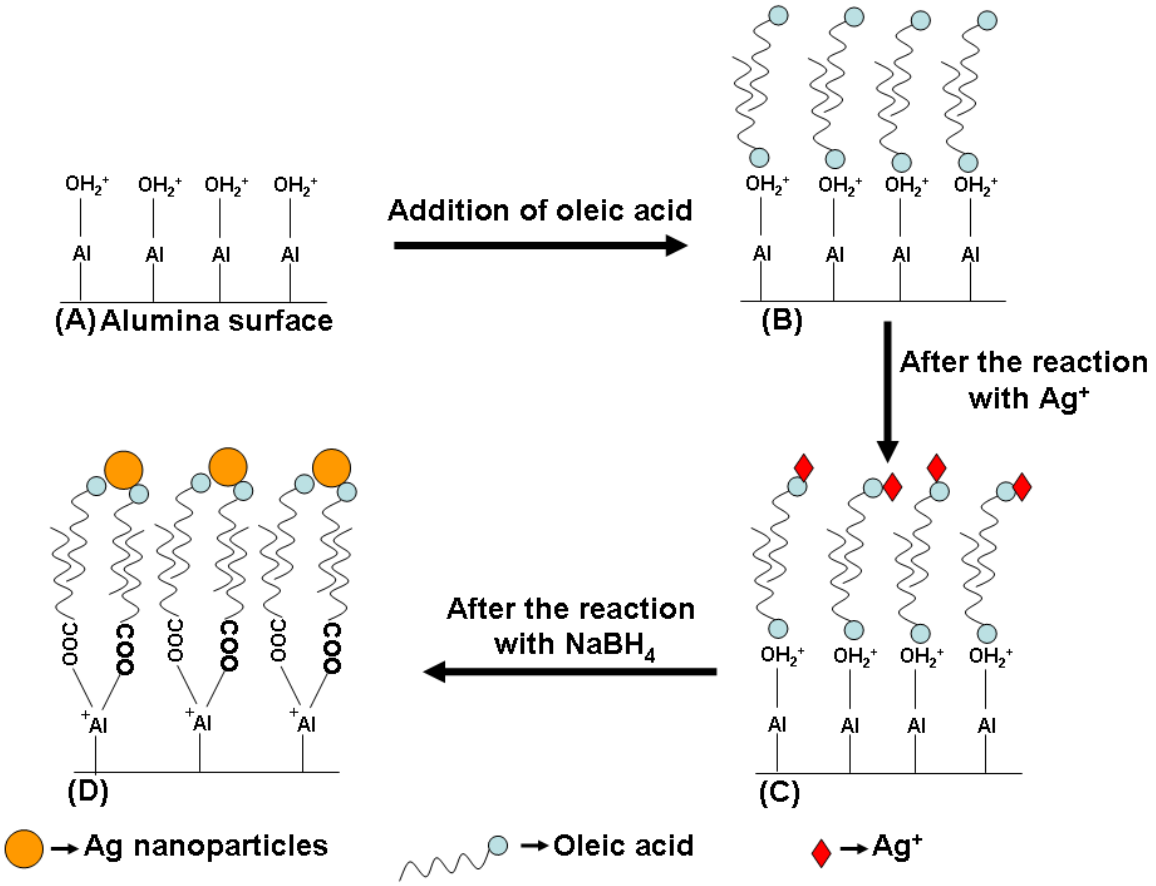


**Scheme 2.** Mode of assembly of $Al_2O_3$–Ag composite nanoparticles. The role of oleic acid in the synthesis is indicated.

**Comparison of $TiO_2$–Ag and $Al_2O_3$–Ag modes of assembly.** The coordination of oleic acid with titania and alumina particles occurred following two different modes, such that the binding strength was not equal in either case. This hypothesis was supported by TGA (cf. Figure 7), from which the

amount of oleic acid adsorbed on the surface of titania and alumina was estimated. Two degradation steps were observed for both $TiO_2$–Ag and $Al_2O_3$–Ag, most readily seen from the derivative TG curves shown inset in Fig 7a and 7b. These double desorption steps are in agreement with studies of thermal stability of surfactants on nanoparticle surfaces conducted by Sahoo *et al* [51] and Perez-Diese *et al* [52].

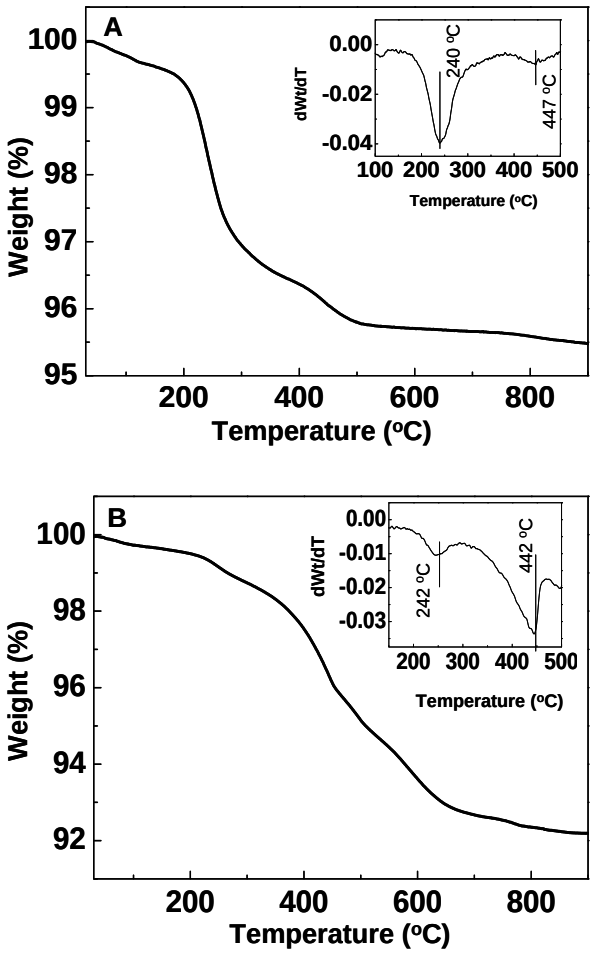


**Figure 7.** (A) TGA trace of $TiO_2$–Ag composite nanoparticles. Inset: derivative curve, showing maximum mass loss at 240 °C. (B) TGA trace of $Al_2O_3$–Ag composite nanoparticles. Inset: derivative curve, showing maximum mass loss at 442 °C.

Desorption of surface bound oleic acid started at 150 ºC for both $TiO_2$–Ag and $Al_2O_3$–Ag. For $TiO_2$–Ag, 3.16 wt% was lost in the first step. The derivative curve (inset, Figure 7A) showed that maximum mass loss occurred at 240 ºC, suggesting that the majority of oleic acid was present as a weakly-bonded layer. A further 0.76 wt% was lost in a second step between 375 ºC and 600 ºC, consistent with desorption of strongly bound oleic acid moieties. Though desorption of weakly-bound oleic acid

also started at 150 ºC for $Al_2O_3$–Ag composite nanoparticles (cf. Figure 7B), the derivative curve (inset, Figure 7B) shows that, unlike $TiO_2$–Ag, the second mass-loss step – attributed to strongly bound surfactant – was dominant. Just 1.01 wt% was lost between 150 ºC and 300 ºC, whereas 2.63 wt% was lost from 300 ºC to 475 ºC. These results are consistent with the modes of assembly outlined in Scheme 1 for $TiO_2$–Ag and Scheme 2 for $Al_2O_3$–Ag.

The stronger interaction between oleic acid and alumina compared to titania might seem to contradict TEM results, whereby loose Ag nanoparticles were more abundant in samples of $Al_2O_3$-Ag composites than $TiO_2$–Ag. This may be explained satisfactorily by considering the proposed modes of assembly. From Scheme 1, a single layer of oleic acid interacts directly with the titania surface. The Ag nanoparticles were directly bound to this layer, preventing easy detachment from the oxide under normal conditions. In contrast, it is hypothesised that, though the inner layer of oleic acid illustrated in Scheme 2 was bonded to alumina strongly, the outer layer was less strongly bound. Thus Ag nanoparticles which were anchored to the oxide surface via this outer layer detached easily. These differences may also account for the more site-specific nanoparticle growth observed for the titania surface.

**Preliminary applications trials.** Preliminary experiments were conducted to evaluate the potential of the $TiO_2$–Ag and $Al_2O_3$–Ag composite nanoparticles for use in formulating antimicrobial materials. A standard epoxy formulation was adopted throughout to allow comparisons of the polymer nanocomposites' relative performance to be made. Specimens containing 10 wt% $TiO_2$–Ag and 10 wt% $Al_2O_3$–Ag composite nanoparticles were formulated at loadings of 1 wt%, 10 wt%, 30 wt% and 50 wt%.

Representative TEM micrographs of the epoxy-based polymer nanocomposites are presented in Figure 8; a specimen of each formulation is shown in the inset photographs. At all loadings prepared, the composite nanoparticles were found to be well dispersed in the epoxy matrix.

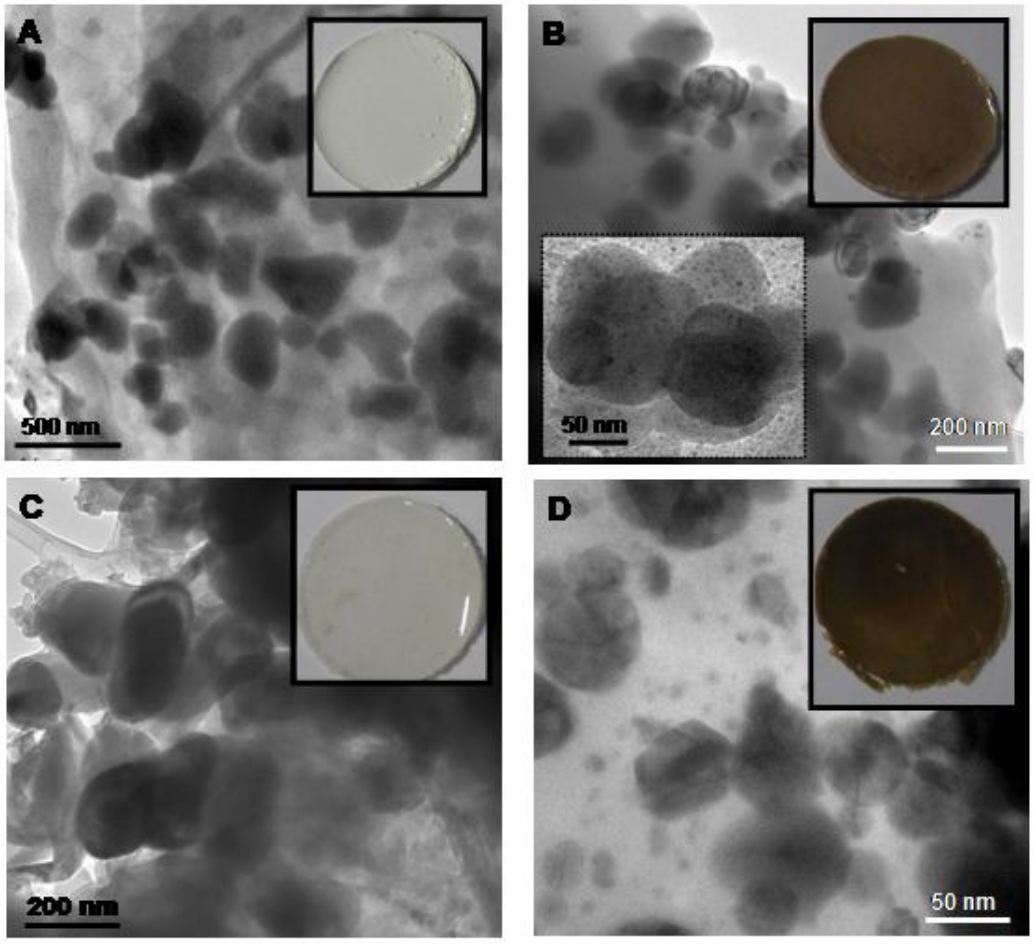


**Figure 8.** (A) TEM image of $TiO_2$/epoxy nanocomposite. (B) TEM image of $TiO_2$-Ag/epoxy nanocomposite. Inset, bottom left: Ag nanoparticles present on titania surface within epoxy matrix. (C) TEM image of $Al_2O_3$/epoxy nanocomposite. (D) TEM image of $Al_2O_3$-Ag/epoxy nanocomposite. For each epoxy nanocomposite formulated, a specimen of the cured formulation is shown inset.

Comparing Figure 8A (50 wt% pristine titania in epoxy) and Figure 8B (50 wt% $TiO_2$-Ag in epoxy), it may be seen that comparable dispersion was achieved in both cases. Similar results were obtained for pristine alumina (cf. Figure 8C) and $Al_2O_3$–Ag composite nanoparticles (cf. Figure 8D). Discrete Ag nanoparticles were clearly observed on the titania surface throughout the epoxy nanocomposite samples (inset, Figure 8B). In contrast, fewer Ag nanoparticles were observed on the surface of the alumina particles dispersed in the epoxy matrix, although unbound Ag nanoparticles were observed in the matrix as may be seen in Figure 8D. Both findings are consistent with the TEM study of neat $TiO_2$-Ag and $Al_2O_3$-Ag.

**Antimicrobial activity.** The antimicrobial properties of both the $TiO_2$–Ag and $Al_2O_3$–Ag containing epoxy nanocomposites were tested against representative Gram negative (*E. coli*) and Gram positive (*S. epidermidis*) bacteria. Discs of epoxy composite loaded with pristine titania created approximately 7mm zones of inhibition when tested against both *E. coli* and *S. epidermidis* (cf. Table 1). Substituting $TiO_2$–10 wt% Ag into this formulation increased the zones of inhibition for both organisms. Only *S. epidermidis* was inhibited by epoxy composite loaded with pristine alumina. However, when $Al_2O_3$–10 wt% Ag was substituted in this formulation, inhibition of both organisms was achieved. Representative examples of the disc diffusion tests are shown in Figure 9, below. To date, no further effort has been made to optimise the epoxy nanocomposite formulation as the optimal formulation will differ based on the target application and selection of epoxy resin used to prepare the nanocomposite.

**Table 1:** Zones of inhibition observed for 6 mm diameter discs of epoxy nanocomposite samples during disc diffusion testing. All nanocomposite samples were formulated with 50 wt% nanoparticles in epoxy matrix.

| **Zone of inhibition (mm)** | ***E. Coli*** | ***S. Epidermis*** |
|---|---|---|
| TiO2/ | 7.65 | 7.03 |
| TiO2–10 wt% Ag | 9.04 | 10 |
| Al2O3 | Not observed | 6.97 |
| Al2O3–10 wt% Ag | 10.76 | 12.25 |

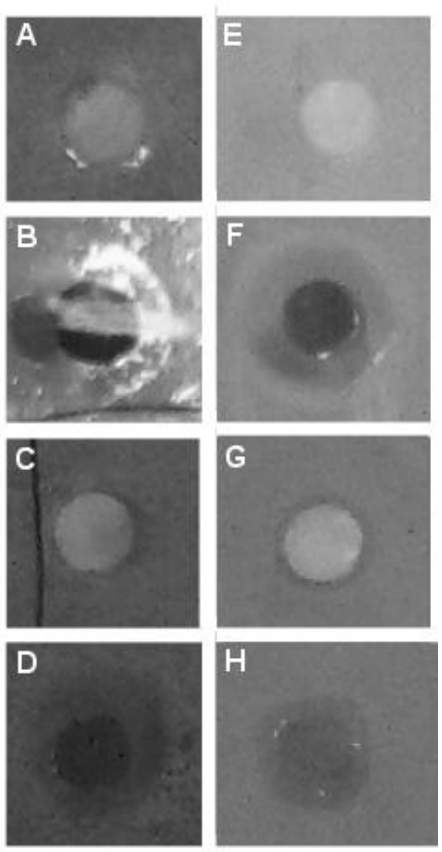


**Figure 9.** Representative agar plates from disc diffusion tests of epoxy nanocomposites prepared at 50 wt% nanoparticle loading. Left column: *S. epidermidis*; (A) Pristine alumina, (B) $Al_2O_3$–10 wt% Ag, (C) pristine titania, (D) $TiO_2$–10 wt% Ag. Right column: *E. coli*.; (E) Pristine alumina, (F) $Al_2O_3$–10 wt% Ag, (G) pristine titania, (H) $TiO_2$–10 wt% Ag. Zones of inhibition observed for each formulation tested are reported in Table 1.

## 4. Conclusions

$TiO_2$-Ag and $Al_2O_3$-Ag composite nanoparticles were prepared using a simple experimental set-up at high yield under ambient conditions with consistent distribution of Ag nanoparticles onto the oxide surface between successive batches of $TiO_2$-Ag and $Al_2O_3$-Ag material. Site-selective reduction of Ag was achieved by using oleic acid as the primary absorbate on the oxide surface. The mode of assembly was elucidated for both materials; though the same linker molecules were used for both the composite preparation, the coordination of oleic acid with alumina and titania was found to differ. The synthesis of $TiO_2$–Ag was considered more successful than that of $Al_2O_3$–Ag, considering the site selective formation of Ag nanoparticles on the surface of the bare oxides achieved. In addition, this

versatile method can reasonably be expected to work for other metallic nanoparticles, such as Ni, Co or Pt, for use as catalysts.

Preliminary applications tests showed that nanocomposites of the $TiO_2$–Ag and $Al_2O_3$–Ag composite nanoparticles dispersed in an epoxy matrix exhibited promising antimicrobial activity. This finding is of increasing relevance given the current need for more effective methods to control microbial infection. Future work will address the optimisation of the polymer matrix selection and nanocomposite formulation to enhance their potential as antimicrobial, catalytic and thermal interface materials.

**Acknowledgement**

The authors thank Dr. Manuel Reuther, School of Chemistry, Trinity College Dublin (TCD) for assistance with thermogravimetric analysis and Dr. Ronald Russell, Moyne Institute, TCD for useful discussions. TB and GA acknowledge financial support from Enterprise Ireland's Commercialisation Fund – Proof of Concept Phase, grant no. PC/2007/117. This work was enabled under the framework of the INSPIRE programme, funded by the Irish Government's Programme for Research in Third Level Institutions, Cycle 4, National Development Plan 2007-2013.

**Supporting Information**

XPS curves for pristine titania particles and $TiO_2$ modified with oleic acid (Figure SI-1), FTIR spectra of oleic acid (Figure SI-2), and XPS curves for pristine alumina particles and $Al_2O_3$ modified with oleic acid (Figure SI-3) are presented as supporting information. This material is available free of charge via the journal website.

**References**

[1] R.J. Davis, M. Boudart, J. Phys. Chem. 98 (1994) 5471.

[2] V.G. Pol, A. Gedanken, J. Calderro-Moreno, Chem. Mater. 15 (2003) 1111.

[3] Z. Konya, V.F. Puntes, I. Kiricsi, J. Zhu, A.P. Alivisatos, G.A. Somorjai, Nano Lett. 2 (2002) 907.

[4] M.R. Hoffmann, S.T. Martin, W. Choi, D.W. Bahnemann, Chem. Rev. 95 (1995) 69.

[5] W.R. Moser, Advanced Catalysis and Nanostructured Materials. Academic Press, San Diego, 1990.

[6] P.V. Kamat, J. Phys. Chem. B 106 (2002) 7729.

[7] M.K. Nazeeruddin, A. Kay, I. Rodicio, R. Humphry-Baker, E. Muller, P. Liska, N. Vlachopoulos, M. Gratzel, J. Am. Chem. Soc. 115 (1993) 6382.

[8] B. O'Regan, M. Gratzel, Nature 353 (1991) 737.

[9] A.J. Bard, M.A. Fox, Acc. Chemistry Research 28 (1995) 141.

[10] A. Fujishima, K. Honda, Nature 37 (1972) 238.

[11] V. Rodríguez-González, E. Marceau, P. Beaunier, M. Che, C. Train, J. Solid State Chem. 180 (2007) 22.

[12] J.L. Contreras, G.A. Fuentes, B. Zeifert, J. Salmones, J. Alloy Compd. 483 (2009) 371.

[13] S. Domínguez-Domínguez, Á. Berenguer-Murcia, Á. Linares-Solano, D. Cazorla-Amorós, J. Catal. 257 (2008) 87.

[14] I. Balint, A. Miyazaki, K.-I. Aika, J. Catal. 220 (2003) 74.

[15] C. Winkler, A.J. Carew, S. Haq, R. Raval, Langmuir 19 (2003) 717.

[16] A. Esteban-Cubillo, C. Díaz, A. Fernández, L.A. Díaz, C. Pecharromán, R. Torrecillas, J.S. Moya, J. Eur. Ceram. Soc. 26 (2006) 1.

[17] S. Sakthivel, M.V. Shankar, M. Palanichamy, B. Arabindoo, D.W. Bahnemann, V. Murugesan, Water Res. 38 (2004) 3001.

[18] B. Kasprzyk-Hordern, Adv. Colloid Interface Sci. 110 (2004) 19.

[19] X. Wang, D.R.G. Mitchell, K. Prince, A.J. Atanacio, R.A. Caruso, Chem. Mater. 20 (2008) 3917.

[20] H. Zhang, G. Wang, D. Chen, X. Lv, J. Li, Chem. Mater. 20 (2008) 6543.

[21] H. Sakai, T. Kanda, H. Shibata, T. Ohkubo, M. Abe, J. Am. Chem. Soc. 128 (2006) 4944.

[22] S.-H. Lee, D.J. Suh, T.-J. Park, K.-L. Kim, Catal. Commun. 3 (2002) 441.

[23] S. Rana, J. Rawat, M.M. Sorensson, R.D.K. Misra, Acta Biomaterialia 2 (2006) 421.

[24] Y. Shen, J. Bao, N. Dai, J. Wu, F. Gu, J.C. Tao, J.C. Zhang, Appl. Surf. Sci. 255 (2009) 3908.

[25] S. Ji, S. Murakami, M. Kamitakahara, K. Ioku, Mater. Res. Bull. 44 (2009) 768.

[26] Y. Yang, Y. Wang, Z. Wang, G. Liu, W. Tian, Mater. Sci. Eng. A 490 (2008) 457.

[27] Y. Wan, J. Ma, W. Zhou, Y. Zhu, X. Song, H. Li, Appl. Catal. A 277 (2004) 55.

[28] Z. Li, B. Hou, Y. Xu, D. Wu, Y. Sun, W. Hu, F. Deng, J. Solid State Chem. 178 (2005) 1395.

[29] Y. Xie, L. Zhou, C. Huang, H. Huang, J. Lu, Electrochim. Acta 53 (2008) 3643.

[30] H. Kong, J. Jang, Biomacromolecules 9 (2008) 2677.

[31] D. Guin, S.V. Manorama, J.N.L. Latha, S. Singh, J. Phys. Chem. C 111 (2007) 13393.

[32] I.M. Arabatzis, T. Stergiopoulos, M.C. Bernard, D. Labou, S.G. Neophytides, P. Falaras, Appl. Catal. B 42 (2003) 187.

[33] Y. Ohko, T. Tatsuma, T. Fujii, K. Naoi, C. Niwa, Y. Kubota, A. Fujishima, Nature Materials 2 (2003) 29.

[34] K. Naoi, Y. Ohko, T. Tatsuma, J. Am. Chem. Soc. 126 (2004) 3664.

[35] V. Subramanian, E.E. Wolf, P.V. Kamat, J. Am. Chem. Soc. 126 (2004) 4943.

[36] P.D. Bragg, D.J. Rainnie, Can. J. Microbiol. 20 (1974) 883.

[37] A.W. Bauer, K.W. M., J.C. Sherris, M. Turck, Am. J. Clin. Pathol. 45 (1966) 93.

[38] http://www.lasurface.com/database/elementxps.php.

[39] D. Briggs, M.P. Seah, Practical Surface Analysis ,Vol. 1, second edition. John Willey & Sons, 1993.

[40] A.E. Miller, C. Ernsberger, D. Banks, J. Nickerson, T. Smith, J. Vac. Sci. Technol. A 4 (1986) 2784.

[41] A. Malagutti, H. Mourao, J. Garbin, C. Ribeiro, Appl. Catal. B 90 (2009) 205.

[42] K.M. Reddy, C.V. Gopal Reddy, S.V. Manorama, J. Solid State Chem. 158 (2001) 180.

[43] P.J. Thistlethwaite, M.S. Hook, Langmuir 16 (2000) 4993.

[44] T. Bala, A. Swami, B.L.V. Prasad, M. Sastry, J. Colloid Interface Sci. 283 (2005) 422.

[45] W. Wang, S. Efrima, O. Regev, Langmuir 14 (1998) 602.

[46] W. Wang, X. Chen, S. Efrima, J. Phys. Chem. B 103 (1999) 7238.

[47] NIST-XPS database, version 3.5 (http://srdata.nist.gov/xps/).

[48] J.F. Moulder, W.F. Stickle, P.E. Sobol, K.D. Bomben, Handbook of X-Ray Photoelectron Spectroscopy. Perkin-Elmer Corporation Physical Electronics Division, 1992.

[49] C. Dablemont, P. Lang, C. Mangeney, J.-Y. Piquemal, V. Petkov, F. Herbst, G. Viau, Langmuir 24 (2008) 5832.

[50] R.M. Silverstein, F.X. Webster, D.J. Kiemle, Spectrometric Identification of Organic Compounds. John Wiley & Sons, Hobokem, NJ, 2005.

[51] Y. Sahoo, H. Pizem, T. Fried, D. Golodnitsky, L. Burstein, C.N. Sukenik, G. Markovich, Langmuir 17 (2001) 7907.

[52] V. Perez-Dieste, O.M. Castellini, J.N. Crain, M.A. Eriksson, A. Kirakosian, J.L. Lin, J.L. McChesney, F.J. Himpsel, C.T. Black, C.B. Murray, Appl. Phys. Lett. 83 (2003) 5053.